INTERNATIONAL JOURNAL FOR NUMERICAL METHODS IN FLUIDS
Int. J. Numer. Meth. Fluids 2010; **62**:574–590
Published online 1 April 2009 in Wiley InterScience (www.interscience.wiley.com). DOI: 10.1002/fld.2037

Internal waves in a two-layer system using fully nonlinear internal-wave equations

K. Nakayama[1,*,†] and T. Kakinuma[2]

[1]*Kitami Institute of Technology, 165 Koen-cho, Kitami City, Japan*
[2]*Kagoshima University, 1-21-40 Korimoto, Kagoshima City, Japan*

SUMMARY

In order to understand the nonlinear effect in a two-layer system, fully nonlinear strongly dispersive internal-wave equations, based on a variational principle, were proposed in this study. A simple iteration method was used to solve the internal-wave equations in order to solve the equations stably. The applicability of the proposed numerical computation scheme was confirmed to agree with linear dispersion relation theoretically obtained from variational principle. The proposed computational scheme was also shown to reproduce internal waves including higher-order nonlinear effect from the analysis of internal solitary waves in a two-layer system. Furthermore, for the second-order numerical analysis, the balance of nonlinearity and dispersion was found to be similar to the balance assumed in the KdV theory and the Boussinesq-type equations. Copyright © 2009 John Wiley & Sons, Ltd.

Received 1 August 2007; Revised 18 November 2008; Accepted 6 February 2009

KEY WORDS: internal waves; variational principle; fully nonlinear; strong dispersivity; internal solitary wave; dispersion relation

1. INTRODUCTION

In a lake or an ocean where density stratification is well developed, the density fluctuation due to a tide or wind generates large amplitude internal waves [1–3]. The first mode of internal waves induces a strong current over the lake or ocean bottom. Such internal waves exchange their energy among components over a wide wave-frequency band, with strong nonlinearity especially when they reach shallow water regions. For example, it has been shown that internal waves and mixing drive residual circulation that may transport dissolved material to the center of a lake [4, 5]. Therefore, it is significant to understand how internal waves are deformed due to the nonlinearity, as well as to clarify the formation of strong current due to the deformation of internal waves.

*Correspondence to: K. Nakayama, Kitami Institute of Technology, 165 Koen-cho, Kitami City, Japan.
†E-mail: nakayama@mail.kitami-it.ac.jp

A considerable number of field observations have been made in an effort to gain understanding of a role of internal waves in lakes, fjords, and coastal regions resulting from internal waves [6, 7]. Since internal waves are deformed in a shallow water region where stronger currents can appear, it is necessary to clarify the energy transfer from low-frequency to high-frequency internal waves especially when internal waves do not show breaking. However, it is hard to obtain field data of spatially high resolution through observations. Theoretical analyses and numerical computations have thus been considered as useful tools to examine the influence of internal waves on flow fields [8–10].

In order to understand the nonlinear effect in a two-layer system, theoretical studies of solitary internal waves, based on the Korteweg-de Vries (KdV) equation or an extended KdV equation, have been carried out (e.g. Holloway *et al*. [11], Horn *et al.* [12]). The formation and propagation of internal solitary waves have been previously discussed by comparing field observations and results from a theoretical model of waves moving onto a continental shelf [11]. The form and rate of steepening of internal waves were found to be strong functions of the coefficient of nonlinearity in the KdV equation. Horn *et al.* [12] also described the importance of nonlinear effects on steepening of internal waves using a steepening time scale obtained from the KdV equation.

The nonlinearity and dispersion of internal waves, however, have been closely studied for internal long waves only. For example, on a perturbation basis, Choi and Camassa [13] derived two sets of internal-wave equations considering full nonlinearity of internal waves in a two-layer system, where one set of equations is chosen to treat a shallow layer whether it lies on another shallow layer with weak dispersion or a deep layer with intermediate dispersivity. In the other previous studies, Tomasson and Melville [14] presented weakly nonlinear solutions of a set of Boussinesq-type equations for internal waves (see also [15–18]). Grimshaw and Horn *et al.* [19, 20] described the evolution and propagation of internal long waves in water of variable depth, for example, by using a modified KdV equation.

On the other hand, Kakinuma [21] did not use any assumption on nonlinearity, as well as dispersion, of internal waves in the derivation process of nonlinear internal-wave equations based on a variational principle, so that the application of the model is theoretically free from limitations concerning the relative thickness of fluid layers or the frequency band of strongly nonlinear and strongly dispersive internal waves. Numerical solutions of the model, however, have been obtained only up to the second order on the vertical length scale of interface displacement. In this study, an attempt has been made to solve the set of fully nonlinear multilayer equations to simulate internal waves in a two-layer system by considering the third and above orders. The fully nonlinear multilayer equations are reduced to a set of nonlinear equations for a two-layer system between horizontal plates, after which a new computational method is proposed to solve the nonlinear two-layer equations. The proposed computation method has been successfully applied. Three stages are shown to verify computational results as follows: (1) verification using the dispersion relation in a two-layer system, (2) generation of a stable internal solitary wave, and (3) comparison with the theoretical solutions of the KdV equation.

2. FULLY NONLINEAR INTERNAL-WAVE EQUATIONS

2.1. Functional for the variational problem

In order to examine fundamental characteristics of internal waves, the equations derived by Kakinuma [21] for a multilayer system are reduced to a set of nonlinear equations for a two-layer

DOI: 10.1002/fld

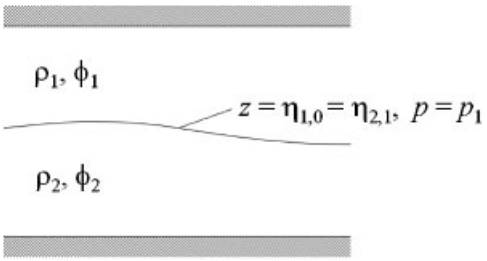

Figure 1. Schematic diagram of multilayer fluid system.

system over a flat bottom below a top wall. Inviscid and incompressible fluids are assumed to be stable in still water, as shown in Figure 1. The upper and lower layers are represented as $m=1$ and 2, respectively. The mth layer thickness in still water is denoted by $h_m(\mathbf{x})$. The two-layer fluids will not mix during the wave motion. The density ρ_m is spatially uniform and temporally constant in each layer, where $\rho_1<\rho_2$. Surface tension and capillary action are neglected. Fluid motion is assumed to be irrotational, resulting in the existence of velocity potential ϕ_m defined as

$$\mathbf{u}_m=\nabla\phi_m \quad \text{and} \quad w_m=\frac{\partial\phi_m}{\partial z} \tag{1}$$

where ∇ is a partial differential operator in the horizontal plane, i.e. $\nabla=(\partial/\partial x, \partial/\partial y)$.

The pressure on $z=\eta_{m,0}$, i.e. the lower interface of the mth layer, is written by $p_m(\mathbf{x},t)$. In the m^{th} layer, if both the elevation of one interface, $z=\eta_{m,1-j}(\mathbf{x},t)$ ($j=0$ or 1), and the pressure on the other interface, $p_{m-j}(\mathbf{x},t)$, are known, then the unknown variables are the velocity potential $\phi_m(\mathbf{x},z,t)$ and interface elevation $z=\eta_{m,j}(\mathbf{x},t)$ such that the functional for the variational problem in the mth layer, F_i, is determined by

$$F_m[\phi_m,\eta_{m,j}] = \int_{t_0}^{t_1}\int\int\int_{\eta_{m,0}}^{\eta_{m,1}}\left\{\frac{\partial\phi_m}{\partial t}+\frac{1}{2}(\nabla\phi_m)^2+\frac{1}{2}\left(\frac{\partial\phi_m}{\partial z}\right)^2+gz+\frac{p_{m-j}+P_m}{\rho_m}\right\}\mathrm{d}z\,\mathrm{d}A\,\mathrm{d}t \tag{2}$$

where $P_m=\sum_{k=1}^{m-1}(\rho_m-\rho_k)gh_k$; g is gravitational acceleration; the plane A, which is the orthogonal projection of the object domain onto the x–y plane is assumed to be independent of time.

In comparison with the functional referred to in Luke [22] for rotational motion, Equation (2) has an additional term of the interfacial pressure without the terms relating to vorticity.

2.2. *Euler–Lagrange equations under variational principle*

In order to derive a set of equations whose type is horizontally two-dimensional, vertical integration is performed analytically. The velocity potential ϕ_m is expanded into a series in terms of a given set of vertically distributed functions, $Z_{m,\alpha}$, multiplied by their weightings, $f_{m,\alpha}$, i.e.

$$\phi_m(\mathbf{x},z,t)=\sum_{\alpha=0}^{N-1} Z_{m,\alpha}(z,h_m(\mathbf{x}))\,f_{m,\alpha}(\mathbf{x},t)\equiv Z_{m,\alpha}f_{m,\alpha} \tag{3}$$

DOI: 10.1002/fld

where N is the number of vertically distributed functions. Throughout this paper, sum rule of product is applied for Greek characters, α, β, and γ.

The vertically distributed functions are determined by

$$Z_{m,\alpha}=\left\{\left(z+\sum_{k=0}^{m-j}h_k\right)\Big/h_m\right\}^{\alpha} \tag{4}$$

where h_0 is defined to be zero. We substitute Equation (3) into Equation (2), after which the functional F_m is integrated vertically. Then the variational principle is applied to obtain the following Euler–Lagrange equations for each layer, i.e. the equations for strongly nonlinear and strongly dispersive internal waves, which we call fully nonlinear and strongly dispersive internal-wave equations (fully nonlinear SDI equations).

1st layer: In the 1st layer, i.e. the upper layer, $m=1$ and $j=1$. We introduce ζ defined as

$$\zeta=\frac{\eta+h_1}{h_1} \tag{5}$$

The Euler–Lagrange equations of the present variational problem are

$$\zeta^{\alpha}\frac{\partial\zeta}{\partial t}+\frac{1}{\alpha+\beta+1}\nabla\{(\zeta^{\alpha+\beta+1}-1)\nabla f_{1,\beta}\}-\frac{1}{h_1^2}\frac{\alpha\beta}{\alpha+\beta-1}(\zeta^{\alpha+\beta-1}-1)f_{1,\beta}=0 \tag{6}$$

$$\zeta^{\beta}\frac{\partial f_{1,\beta}}{\partial t}+\frac{1}{2}\zeta^{\beta+\gamma}\nabla f_{1,\beta}\nabla f_{1,\gamma}+\frac{1}{2}\frac{\beta\gamma}{h_1^2}\zeta^{\beta+\gamma-2}f_{1,\beta}f_{1,\gamma}+g\eta+\frac{p_1}{\rho_1}=0 \tag{7}$$

where $\alpha=0,1,2,\ldots,N-1$.

2nd layer: In the 2nd layer, i.e. the lower layer, $m=2$ and $j=0$. We introduce ξ defined as

$$\xi=\frac{\eta+h_1}{h_2} \tag{8}$$

The Euler–Lagrange equations become

$$\xi^{\alpha}\frac{\partial\xi}{\partial t}+\frac{1}{\alpha+\beta+1}\nabla\{[\xi^{\alpha+\beta+1}-(-1)^{\alpha+\beta+1}]\nabla f_{2,\beta}\}-\frac{1}{h_2^2}\frac{\alpha\beta}{\alpha+\beta-1}\{\zeta^{\alpha+\beta-1}-(-1)^{\alpha+\beta-1}\}f_{2,\beta}=0 \tag{9}$$

$$\xi^{\beta}\frac{\partial f_{2,\beta}}{\partial t}+\frac{1}{2}\xi^{\beta+\gamma}\nabla f_{2,\beta}\nabla f_{2,\gamma}+\frac{1}{2}\frac{\beta\gamma}{h_2^2}\zeta^{\beta+\gamma-2}f_{1,\beta}f_{2,\gamma}+g\eta+\frac{p_1+(\rho_2-\rho_1)gh_1}{\rho_2}=0 \tag{10}$$

where $\alpha=0,1,2,\ldots,N-1$.

3. COMPUTATIONAL METHOD

Equations (5)–(10) can provide solutions for internal waves over a flat bottom under the condition of rigid wall on water surfaces. This study aims to verify the validity of numerical computation

DOI: 10.1002/fld

scheme for one-dimensional propagation problem. To obtain stable computational results, implicit technique is used in the proposed numerical computational scheme.

$$(\zeta^n)^\alpha \frac{\zeta_i^{n+1}-\zeta_i^n}{\Delta t} + (\zeta^n)^{\alpha+\beta} \frac{\zeta_{i+1}^n-\zeta_{i-1}^n}{2\Delta x} \frac{f_{1,\beta,i+1}^{n+1}-f_{1,\beta,i-1}^{n+1}}{2\Delta x} + \frac{(\zeta_i^n)^{\alpha+\beta+1}-1}{\alpha+\beta+1} \frac{f_{1,\beta,i+1}^{n+1}+f_{1,\beta,i-1}^{n+1}-2f_{1,\beta,i}^{n+1}}{(\Delta x)^2} - \frac{1}{h_1^2}\frac{\alpha\beta}{\alpha+\beta-1}\{(\zeta_i^n)^{\alpha+\beta-1}-1\} f_{1,\beta,i}^{n+1} = 0 \tag{11}$$

$$(\zeta_i^n)^\beta \frac{f_{1,\beta,i}^{n+1}-f_{1,\beta,i}^n}{\Delta t} + \frac{1}{2}(\zeta_i^n)^{\beta+\gamma} \frac{f_{1,\beta,i+1}^{n+1}-f_{1,\beta,i-1}^{n+1}}{2\Delta x} \frac{f_{1,\gamma,i+1}^n-f_{1,\gamma,i-1}^n}{2\Delta x} + \frac{1}{2}\frac{\beta\gamma}{h_1^2}(\zeta_i^n)^{\beta+\gamma-2} f_{1,\beta,i}^{n+1} f_{1,\gamma,i}^n + g\eta_i^{n+1} + \frac{p_{1,i}^{n+1}}{\rho_1} = 0 \tag{12}$$

$$(\xi^n)^\alpha \frac{\xi_i^{n+1}-\xi_i^n}{\Delta t} + (\xi^n)^{\alpha+\beta} \frac{\xi_{i+1}^n-\xi_{i-1}^n}{2\Delta x} \frac{f_{2,\beta,i+1}^{n+1}-f_{2,\beta,i-1}^{n+1}}{2\Delta x} + \frac{(\xi_i^n)^{\alpha+\beta+1}-1}{\alpha+\beta+1} \frac{f_{2,\beta,i+1}^{n+1}+f_{2,\beta,i-1}^{n+1}-2f_{2,\beta,i}^{n+1}}{(\Delta x)^2} - \frac{1}{h_2^2}\frac{\alpha\beta}{\alpha+\beta-1}\{(\xi_i^n)^{\alpha+\beta-1}-1\} f_{2,\beta,i}^{n+1} = 0 \tag{13}$$

$$(\xi_i^n)^\beta \frac{f_{2,\beta,i}^{n+1}-f_{2,\beta,i}^n}{\Delta t} + \frac{1}{2}(\xi_i^n)^{\beta+\gamma} \frac{f_{2,\beta,i+1}^{n+1}-f_{2,\beta,i-1}^{n+1}}{2\Delta x} \frac{f_{2,\gamma,i+1}^n-f_{2,\gamma,i-1}^n}{2\Delta x} + \frac{1}{2}\frac{\beta\gamma}{h_2^2}(\xi_i^n)^{\beta+\gamma-2} f_{2,\beta,i}^{n+1} f_{2,\gamma,i}^n + g\eta_i^{n+1} + \frac{p_{1,i}^{n+1}+(\rho_2-\rho_1)gh_1}{\rho_2} = 0 \tag{14}$$

It should be noted that the suffix i indicates the grid-point number in Equations (11)–(14). To obtain the solutions of Equations (11)–(14), the matrix whose number of column is (number of grids) $\times(2N+2)$ has to be solved. $(2N+2)$ is the number of equations generated from Equations (11)–(14). It would not be a big problem to solve such a matrix for one-dimensional propagation problem. However, the cost would be very expensive and it would not be practical when two-dimensional propagation problem was dealt. Therefore, we propose the scheme in which an

DOI: 10.1002/fld

iterational method is used to obtain solutions for each node of the grids. When the number of the step of iteration is defined as k, the matrix on the step of $k+1$ is indicated as follows:

$$\begin{pmatrix} C_{1,1} & \cdots & C_{1,N} & C_{1,N+1} & 0 & 0 & 0 & 0 \\ \vdots & \ddots & \vdots & \vdots & 0 & 0 & 0 & 0 \\ C_{N,1} & \cdots & C_{N,N} & C_{N,N+1} & 0 & 0 & 0 & 0 \\ C_{N+1,1} & \cdots & C_{N+1,N} & C_{N+1,N+1} & C_{N+1,N+2} & 0 & 0 & 0 \\ 0 & 0 & 0 & C_{N+2,N+1} & C_{N+2,N+2} & C_{N+2,N+3} & \cdots & C_{N+2,2N+2} \\ 0 & 0 & 0 & C_{N+3,N+1} & 0 & C_{N+3,N+3} & \cdots & C_{N+3,2N+2} \\ 0 & 0 & 0 & \vdots & 0 & \vdots & \ddots & \vdots \\ 0 & 0 & 0 & C_{2N+2,N+1} & 0 & C_{2N+2,N+3} & \cdots & C_{2N+2,2N+2} \end{pmatrix}$$

$$\times \begin{pmatrix} (f_{1,0,i}^{n+1})^{k+1} \\ \vdots \\ (f_{1,N-1,i}^{n+1})^{k+1} \\ (\zeta_i^{n+1})^{k+1} \\ (P_{1,i}^{n+1})^{k+1} \\ (f_{2,0,i}^{n+1})^{k+1} \\ \vdots \\ (f_{2,N-1,i}^{n+1})^{k+1} \end{pmatrix} = \begin{pmatrix} D_1 \\ \vdots \\ D_N \\ D_{N+1} \\ D_{N+2} \\ D_{N+3} \\ \vdots \\ D_{2N+2} \end{pmatrix} \tag{15}$$

$$C_{\alpha+1,\beta+1} = \frac{(-2)}{(\Delta x)^2} \frac{(\zeta_i^n)^{\alpha+\beta+1} - 1}{\alpha+\beta+1} - \frac{1}{h_1^2} \frac{\alpha\beta}{\alpha+\beta-1} \{(\zeta_i^n)^{\alpha+\beta-1} - 1\} \quad \begin{pmatrix} \alpha = 0, \ldots, N-1 \\ \beta = 0, \ldots, N-1 \end{pmatrix} \tag{16}$$

$$C_{\alpha+1,N+1} = \frac{(\zeta^n)^\alpha}{\Delta t} \ (\alpha = 0, \ldots, N-1) \tag{17}$$

$$C_{N+1,\beta+1} = \frac{(\zeta_i^n)^\beta}{\Delta t} + \sum_{\gamma=1}^{N-1} \frac{1}{2} \frac{\beta\gamma}{h_1^2} (\zeta_i^n)^{\beta+\gamma-2} (f_{1,\gamma,i}^n)^k \quad (\beta = 0, \ldots, N-1) \tag{18}$$

$$C_{N+1,N+1} = gh_1 \tag{19}$$

$$C_{N+1,N+2} = \frac{1}{\rho_1} \tag{20}$$

$$C_{N+2,N+1} = gh_1 \tag{21}$$

DOI: 10.1002/fld

$$C_{N+2,N+2}=\frac{1}{\rho_2} \tag{22}$$

$$C_{N+2,N+\beta+3}=\frac{(\xi_i^n)^\beta}{\Delta t}+\sum_{\gamma=1}^{N-1}\frac{1}{2}\frac{\beta\gamma}{h_2^2}(\xi_i^n)^{\beta+\gamma-2}(f_{2,\gamma,i}^n)^k \ (\beta=0,\ldots,N-1) \tag{23}$$

$$C_{N+\alpha+3,N+\beta+3}=\frac{(-2)}{(\Delta x)^2}\frac{(\xi_i^n)^{\alpha+\beta+1}-1}{\alpha+\beta+1}-\frac{1}{h_2^2}\frac{\alpha\beta}{\alpha+\beta-1}\{(\xi_i^n)^{\alpha+\beta-1}-1\} \quad \begin{pmatrix}\alpha=0,\ldots,N-1\\ \beta=0,\ldots,N-1\end{pmatrix} \tag{24}$$

$$C_{N+\alpha+3,N+1}=\frac{h_1}{h_2}\frac{(\xi^n)^\alpha}{\Delta t} \quad (\alpha=0,\ldots,N-1) \tag{25}$$

$$D_{\alpha+1}=(\zeta^n)^\alpha\frac{\zeta_i^n}{\Delta t}-\sum_{\beta=0}^{N-1}(\zeta^n)^{\alpha+\beta}\frac{\zeta_{i+1}^n-\zeta_{i-1}^n}{2\Delta x}\frac{(f_{1,\beta,i+1}^{n+1})^k-(f_{1,\beta,i-1}^{n+1})^k}{2\Delta x}$$
$$-\sum_{\beta=0}^{N-1}\frac{(\zeta_i^n)^{\alpha+\beta+1}-1}{\alpha+\beta+1}\frac{(f_{1,\beta,i+1}^{n+1})^k+(f_{1,\beta,i-1}^{n+1})^k}{(\Delta x)^2} \quad (\alpha=0,\ldots,N-1) \tag{26}$$

$$D_{N+1}=\sum_{\beta=0}^{N-1}(\zeta_i^n)^\beta\frac{f_{1,\beta,i}^n}{\Delta t}-\sum_{\beta=0}^{N-1}\sum_{\gamma=0}^{N-1}\frac{1}{2}(\zeta_i^n)^{\beta+\gamma}\frac{f_{1,\beta,i+1}^{n+1}-f_{1,\beta,i-1}^{n+1}}{2\Delta x}\frac{f_{1,\gamma,i+1}^n-f_{1,\gamma,i-1}^n}{2\Delta x} \tag{27}$$

$$D_{N+2}=\sum_{\beta=0}^{N-1}(\xi_i^n)^\beta\frac{f_{2,\beta,i}^n}{\Delta t}$$
$$-\sum_{\beta=0}^{N-1}\sum_{\gamma=0}^{N-1}\frac{1}{2}(\xi_i^n)^{\beta+\gamma}\frac{f_{2,\beta,i+1}^{n+1}-f_{2,\beta,i-1}^{n+1}}{2\Delta x}\frac{f_{2,\gamma,i+1}^n-f_{2,\gamma,i-1}^n}{2\Delta x}-\varepsilon g h_1=0 \tag{28}$$

$$D_{N+\alpha+3}=(\xi^n)^\alpha\frac{\xi_i^n}{\Delta t}-\sum_{\beta=0}^{N-1}(\xi^n)^{\alpha+\beta}\frac{\xi_{i+1}^n-\xi_{i-1}^n}{2\Delta x}\frac{f_{2,\beta,i+1}^{n+1}-f_{2,\beta,i-1}^{n+1}}{2\Delta x}$$
$$-\sum_{\beta=0}^{N-1}\frac{(\xi_i^n)^{\alpha+\beta+1}-(-1)^{\alpha+\beta+1}}{\alpha+\beta+1}\frac{f_{2,\beta,i+1}^{n+1}+f_{2,\beta,i-1}^{n+1}}{(\Delta x)^2} \quad (\alpha=0,\ldots,N-1) \tag{29}$$

The iteration finishes when the values of variables on the step of $k+1$ match to that on the step of k. The proposed numerical computation scheme thus has the following two characteristics of numerical analysis.

(1) The size of the matrix, which has to be solved is smaller than that of normal matrix by introducing the iterational method.
(2) Since non-zero value can be located on a diagonal in a matrix, the matrix can be solved stably.

DOI: 10.1002/fld

4. DISPERSION RELATION

4.1. Dispersion relation from proposed nonlinear internal-wave equations and performance evaluation of numerical computation scheme

In this section, the applicability of the proposed numerical computation scheme was investigated by comparing with dispersion relation obtained from the linearlized fully nonlinear SDI equations (Dispersion relation for surface waves has been derived in the Reference [23] by Isobe.). First, the fully nonlinear SDI equations were linearlized by using a small amplitude assumption in order to derive dispersion relation. In this case, the vertically distributed functions should be:

$$Z_{1,\alpha}=\left(-\frac{z}{h_1}\right)^{\alpha} \quad (m=1 \text{ and } j=1) \tag{30}$$

$$Z_{2,\alpha}=\left(\frac{z+h_1+h_2}{h_2}\right)^{\alpha} \quad (m=2 \text{ and } j=0) \tag{31}$$

$$\int_{\eta}^{0} Z_{1,\alpha}Z_{1,\beta}\,\mathrm{d}z=\frac{h_1}{\alpha+\beta+1} \tag{32}$$

$$\int_{\eta}^{0} \frac{\partial Z_{1,\alpha}}{\partial z}\frac{\partial Z_{1,\beta}}{\partial z}\,\mathrm{d}z=\frac{\alpha\beta}{h_1(\alpha+\beta-1)} \tag{33}$$

$$\int_{-H}^{\eta} Z_{2,\alpha}Z_{2,\beta}\,\mathrm{d}z=\frac{h_2}{\alpha+\beta+1} \tag{34}$$

$$\int_{-H}^{\eta} \frac{\partial Z_{2,\alpha}}{\partial z}\frac{\partial Z_{2,\beta}}{\partial z}\,\mathrm{d}z=\frac{\alpha\beta}{h_2(\alpha+\beta-1)} \tag{35}$$

Then, the equations for linearized internal waves with strong dispersion for the upper and lower layers are derived as:

1st layer:

$$-\frac{\partial\eta}{\partial t}+\frac{h_1}{\alpha+\beta+1}\frac{\partial^2 f_{1,\beta}}{\partial x^2}-\frac{1}{h_1}\frac{\alpha\beta}{\alpha+\beta-1}f_{1,\beta}=0 \tag{36}$$

$$\frac{\partial f_{1,\beta}}{\partial t}+g\eta+\frac{p_1}{\rho_1}=0 \tag{37}$$

2nd layer:

$$\frac{\partial\eta}{\partial t}+\frac{h_2}{\alpha+\beta+1}\frac{\partial^2 f_{2,\beta}}{\partial x^2}-\frac{1}{h_2}\frac{\alpha\beta}{\alpha+\beta-1}f_{2,\beta}=0 \tag{38}$$

$$\frac{\partial f_{2,\beta}}{\partial t}+g\eta+\frac{p_1+(\rho_2-\rho_1)gh_1}{\rho_2}=0 \tag{39}$$

DOI: 10.1002/fld

Equation (40) is obtained from Equations (36) and (38).

$$\frac{1}{\alpha+\beta+1}\frac{\partial^2}{\partial x^2}(h_1 f_{1,\beta}+h_2 f_{2,\beta})-\frac{\alpha\beta}{\alpha+\beta-1}\left(\frac{f_{1,\beta}}{h_1}+\frac{f_{2,\beta}}{h_2}\right)=0 \tag{40}$$

Giving small amplitude internal wave yields the following relations:

$$f_{1,\beta}=F_{1,\beta}\exp\{i(\sigma t-kx)\} \tag{41}$$

$$f_{2,\beta}=F_{2,\beta}\exp\{i(\sigma t-kx)\} \tag{42}$$

$$-\left(\frac{h_1}{\alpha+\beta+1}k^2+\frac{\alpha\beta}{\alpha+\beta-1}\frac{1}{h_1}\right)F_{1,\beta}=\left(\frac{h_2}{\alpha+\beta+1}k^2+\frac{\alpha\beta}{\alpha+\beta-1}\frac{1}{h_2}\right)F_{2,\beta} \tag{43}$$

$$F_{1,\beta}=G_{\beta,\gamma}F_{2,\gamma}=-\begin{pmatrix} h_1k^2 & \cdots & \frac{h_1}{N}k^2 \\ \vdots & \ddots & \vdots \\ \frac{h_1}{N}k^2 & \cdots & \frac{h_1}{2N-1}k^2+\frac{(N-1)(N-1)}{2N-3}\frac{1}{h_1} \end{pmatrix}^{-1} \times\begin{pmatrix} h_2k^2 & \cdots & \frac{h_2}{N}k^2 \\ \vdots & \ddots & \vdots \\ \frac{h_2}{N}k^2 & \cdots & \frac{h_2}{2N-1}k^2+\frac{(N-1)(N-1)}{2N-3}\frac{1}{h_2} \end{pmatrix}F_{2,\gamma} \tag{44}$$

Equations (38)–(40) may be modified as:

$$-\frac{\partial^2 f_{2,\beta}}{\partial t^2}+\frac{\rho_1}{\rho_2}\frac{\partial^2 f_{1,\beta}}{\partial t^2}+\frac{\rho_2-\rho_1}{\rho_2}g\frac{h_2}{\alpha+\beta-1}\frac{\partial^2 f_{2,\beta}}{\partial x^2}-\frac{\rho_2-\rho_1}{\rho_2}\frac{1}{h_2}\frac{\alpha\beta}{\alpha+\beta-1}f_{2,\beta}=0 \tag{45}$$

Substituting Equations (41) and (42) into (45) leads Equation (46).

$$\sigma^2F_{2,\beta}-\sigma^2\frac{\rho_1}{\rho_2}G_{\beta,\gamma}F_{2,\gamma}-\frac{\rho_2-\rho_1}{\rho_2}g\frac{h_2}{\alpha+\beta-1}k^2F_{2,\beta}-\frac{\rho_2-\rho_1}{\rho_2}\frac{1}{h_2}\frac{\alpha\beta}{\alpha+\beta-1}F_{2,\beta}=0 \tag{46}$$

Finally, exchange of dummy subscripts, γ and β, of the second term in the left-hand side of Equation (46) yields dispersion relation shown as Equation (47).

$$-\sigma^2\left(-1+\frac{\rho_1}{\rho_2}G_{\gamma,\beta}\right)-\frac{\rho_2-\rho_1}{\rho_2}g\frac{h_2}{\alpha+\beta-1}k^2-\frac{\rho_2-\rho_1}{\rho_2}\frac{1}{h_2}\frac{\alpha\beta}{\alpha+\beta-1}=0 \tag{47}$$

To investigate how accurately the proposed numerical computational scheme described in Section 3 reproduce the solution of Equation (47), which indicates linearized internal waves with strong dispersion, the comparison was made up to $N=3$ of vertically distributed function. Three cases were chosen, two cases for internal waves and one case for surface waves (Table I and Figure 2). Horizontal axis is normalized by the depth of the lower layer and the wavelength in

DOI: 10.1002/fld

Table I. Conditions for each case.

	$(\rho_2-\rho_1)/\rho_2$	h_1/h_2
Case 1	0.01	1
Case 2	0.01	9
Case 3	0.999	9

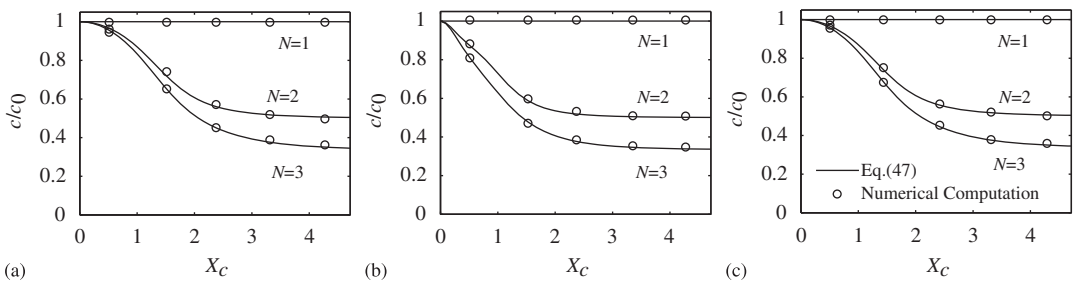

Figure 2. Comparisons of dispersion relation. Solid lines indicate dispersion relation obtained from linearlized internal-wave equations with strong dispersion up to $N=3$. Circles indicate the numerical computational solutions: (a) Case 1; (b) Case 2; and (c) Case 3.

Figure 2, λ, may be obtained from

$$\lambda=\frac{2\pi h_2}{X_c}\left(\frac{c}{c_0}\right) \tag{48}$$

where c_0 is velocity of long wave and X_c is value of x coordinate. The computations were carried out for 15 cases with the ranges of $N=1$, $N=2$ to $N=3$ and $X_c=3\pi/20$, $X_c=9\pi/20$, $X_c=15\pi/20$, $X_c=21\pi/20$ to $X_c=27\pi/20$. The number of grid for one wave was taken as 30 and the computational domain was given equal to the length of nine waves. Progressive waves were given from the left end boundary with a small amplitude. Time step was given by satisfying a condition of CFL$=0.1$, in which celerity is considered representative velocity. The total computational time was taken as four periods of waves, and celerity was obtained from the third propagation wave (Figure 2). The computed celerity fits to that obtained from the linearized internal-wave equations with strong dispersion for all the cases. Therefore, the proposed numerical computation scheme is found to have high applicability of dispersion relation for small amplitude waves.

4.2. Dispersion relation from the linear theory and proposed fully nonlinear SDI equations

In this section, to verify the validity of Equation (47), dispersion relation was investigated by comparing with the theoretical solution of dispersion relation for internal waves. Dispersion relation from the theory is indicated as

$$\sigma^2=\frac{\rho_2 gk}{2}\frac{1}{\rho_2\coth(kh_1)\coth(kh_2)+\rho_1}\left[\coth(kh_1)+\coth(kh_2)\pm\left\{\{\coth(kh_1)+\coth(kh_2)\}^2\right.\right.$$
$$\left.\left.-4\left\{\coth(kh_1)\coth(kh_2)+\frac{\rho_1}{\rho_2}\right\}\frac{\rho_2-\rho_1}{\rho_2}\right\}^{1/2}\right] \tag{49}$$

DOI: 10.1002/fld

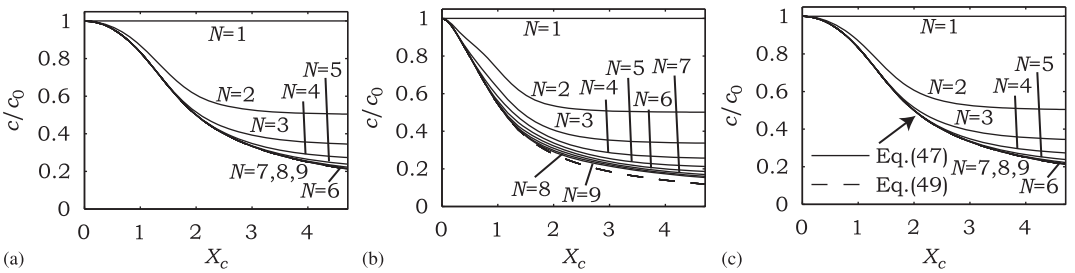

Figure 3. Comparisons of dispersion relation. Solid lines indicate dispersion relation obtained from linearized internal-wave equations with strong dispersion up to $N=9$. Broken lines indicate the theoretical solutions of dispersion relation for internal waves: (a) Case 1; (b) Case 2; and (c) Case 3.

Dispersion relation obtained from variational principle was computed up to $N=9$ (Figure 3). In Case 1 when the upper and lower layer depths are the same for internal wave case, the theoretical solution is found to agree with that obtained from variational principle when $N=6$. When $N=3$, dispersion relation obtained from variational principle agrees well up to $X_c=1.8$ and $c/c_0=0.55$. The ratio of wavelength and the lower layer depth is about 1.9 computed from Equation (47) when $X_c=1.8$ and $c/c_0=0.55$, which reveals that dispersion relation obtained from variational principle can reproduce the characteristics of waves excluding deepwater waves even if $N=3$ is taken for the case when the ratio of depth of the upper and lower layer is 1 for internal waves.

On the other hand, even Case 2 is an internal wave case, dispersion relation obtained from variational principle cannot reproduce the theoretical solution even if N is take up to 9 when the ratio of the depth of the upper and lower layer is 9. The minimum wavelengths that have good agreement with the theoretical solution are obtained as 2.6 and 1.7 for the cases of $N=6$ and $N=7$, respectively. This results may provide the necessity of larger N when the lower layer depth is much less than that of the upper layer for internal wave cases. In Case 3 when the ratio of the depth of the upper and lower layers is 9 for surface waves, dispersion relation obtained from variational principle is found to agree with the theoretical solution very well when $N=6$. In this study, although we proposed power function to indicate velocity potential, it is expected to get much better agreement by introducing different types of functions, like hyperbolic tangent.

5. INTERNAL SOLITARY WAVE

5.1. Initial setup and boundary conditions

In the previous section, the applicability of linear internal-wave equations with strong dispersion obtained from variational principle is revealed to have very good agreement with the theoretical solution. In this section, we thus investigate the applicability of the proposed fully nonlinear SDI equations into an internal solitary wave.

The initial condition was given as shown in Figure 4 in order to generate an internal solitary wave [9, 24]. The total computational domain is 2 m, and the number of mesh is given as 400. The depths of the upper and lower layers are 0.105 and 0.045 m, respectively. The specific density ratio of the upper and lower layer, $(\rho_2-\rho_1)/\rho_2$, is 0.04, and the height of the step-like shape displacement is given as a half of the lower layer depth, which may generate a strongly nonlinear

DOI: 10.1002/fld

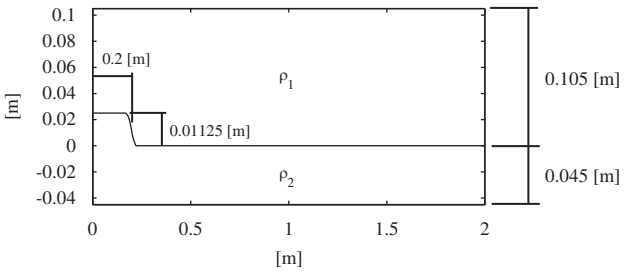

Figure 4. Initial setup for generating an internal solitary wave.

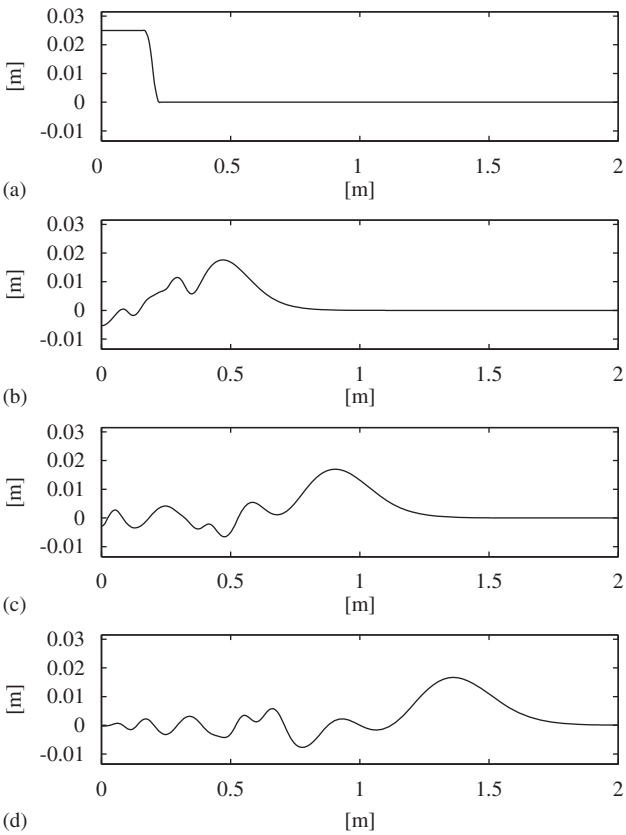

Figure 5. Internal wave generation and propagation at: (a) $t=0$; (b) $t=4$; (c) $t=8$; and (d) $t=12$ s.

internal solitary wave. The time step is taken as 0.02 s. Solid walls are given as boundary conditions for the both ends of the computational domain.

The computational results when $N=6$ are shown in Figure 5 ($t=0$, $t=4$, $t=8$, and $t=12$ s). An internal solitary wave is confirmed to propagate with amplitude of $\frac{1}{3}$ of the lower layer depth. In the

DOI: 10.1002/fld

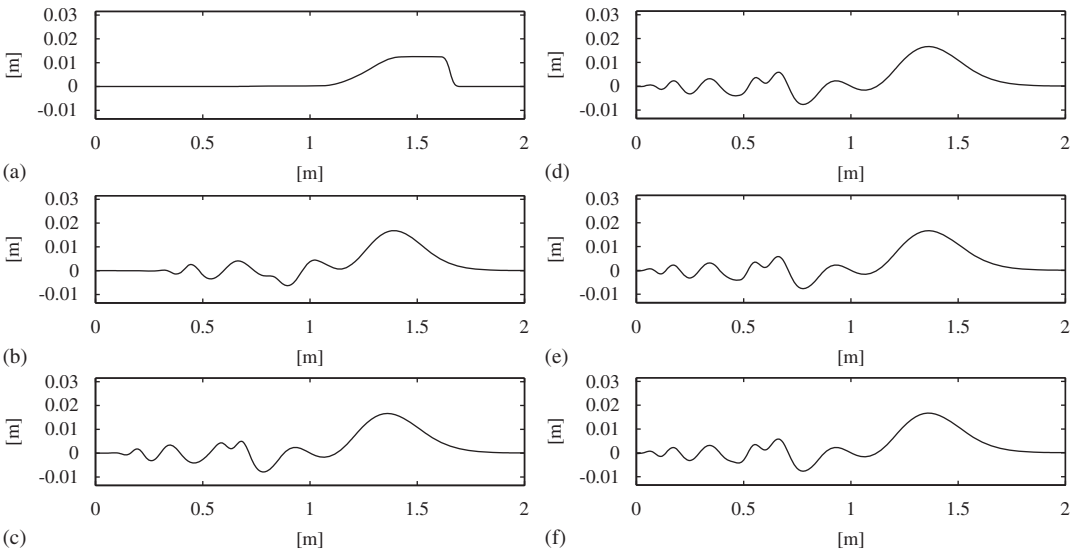

Figure 6. Generated internal waves at $12=0$ s. (a) $N=1$; (b) $N=2$; (c) $N=3$; (d) $N=4$; (e) $N=5$; and (f) $N=6$.

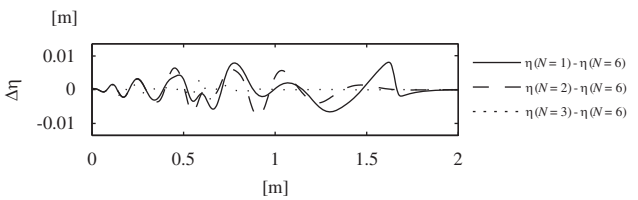

Figure 7. Differences of internal wave displacement from $N=6$. Solid lines indicate $\Delta\eta=\eta_{(N=1)}-\eta_{(N=6)}$. Broken lines indicate $\Delta\eta=\eta_{(N=2)}-\eta_{(N=6)}$. Dotted lines indicate $\Delta\eta=\eta_{(N=3)}-\eta_{(N=6)}$.

tail of the internal solitary wave, there are various types of internal waves with different frequency and amplitude. Since the internal solitary wave has larger amplitude compared with the other internal waves, the internal solitary wave is found to propagate separately with a larger celerity.

Comparisons were made for the cases, $N=1$, 2, 3, to 6, when $t=12$ s (Figures 6 and 7). Since only a long internal wave can exist in the case of $N=1$, clear internal bore was generated. In the case of $N=2$, since the proposed fully nonlinear SDI equations include dispersion relation for weak nonlinearity of the same order as the KdV equation, an internal solitary wave is found to be formed. In the case of $N=3$, there clearly exist differences of the shape of internal waves compared with the case of $N=2$, in particular, in the tail of an internal solitary wave. However, there is of no great difference among the cases of $N=4$ to $N=6$. The minimum wavelength of internal waves was about 0.1 m for all cases. Since the lower layer depth is 0.045 m and the ratio of the wavelength and the lower layer depth is taken to be larger than 2 in this study with the ratio of the upper and lower layers is $\frac{3}{7}$, it is considered that there is no differences in the cases when N is larger than 4 like being expected from Figure 2.

DOI: 10.1002/fld

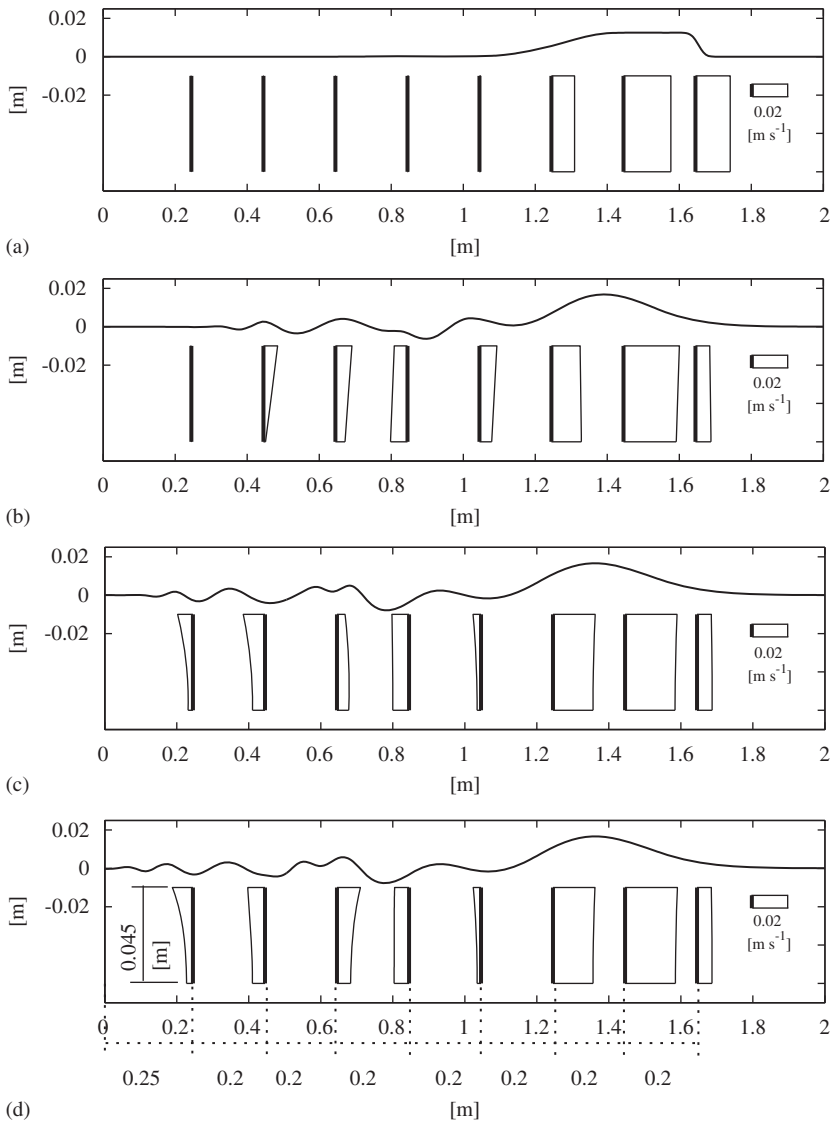

Figure 8. Vertical profile of horizontal velocity with a spatial interval of 0.2 m. (a) $N=1$; (b) $N=2$; (c) $N=3$; and (d) $N=6$.

As there are no large enough differences in the cases when N is larger than 4, the differences of interfacial displacement from the case of $N=6$ were computed for the cases of $N=1$ to $N=3$, respectively (Figure 7). The larger the N, the smaller the difference of interfacial displacement. In particular, the shape of an internal solitary wave agrees well among $N=3$ to $N=6$. In the tail of the internal solitary wave, the difference is the largest around $x=0.4$ m to 1 m where the wavelength is shorter and the amplitude is larger compared with the other internal waves.

DOI: 10.1002/fld

As the vertical profile of horizontal velocity for the cases of $N=4$ to $N=6$ was confirmed to be the same, the profile for the cases of $N=1$, $N=2$, $N=3$, and $N=6$ is only shown in Figure 8. According to the vertical profile of velocity around an internal solitary wave, the functions more than a squared function in the power function do not seem to be significant. However, like mentioned in Figure 7, the functions more than a squared function are important in order to duplicate an internal solitary wave, which means that at least $N=3$ has to be taken into account for reproducing an internal solitary wave dealt with in this study. On the other hand, since the wavelength of internal waves is shorter than the lower layer depth in the tail of the internal solitary wave, it is conceivable that the higher-order functions have to be taken into account. As suggested in the investigation of dispersion relation shown in Figure 2, till what order of the function should be included depends on the problem, such as the ratio of the depth of the upper and lower layers. Therefore, it is needed to deal with each problem based on theoretical consideration, at least, like dispersion relation.

5.2. Comparisons with theoretical solutions

In the previous section, the vertical profile of the horizontal velocity is found to be the same in the cases of that N is larger than three. Thus, the cases of $N=2$ and $N=6$ were only selected to investigate the shape of an internal solitary wave by using KdV theory, which may provide the understanding of what kind of characteristics the internal solitary wave generated in this study has. The shape of an internal solitary wave is given using the following equations:

$$\gamma_1=\frac{3(h_1+h_2)}{2h_1h_2}\left(\frac{-h_1^2\rho_2+h_2^2\rho_1}{\rho_1h_2+\rho_2h_1}\right) \tag{50}$$

$$\gamma_2=\frac{h_1h_2}{6(h_1+h_2)^2}\left(\frac{\rho_1h_1+\rho_2h_2}{\rho_1h_2+\rho_2h_1}\right) \tag{51}$$

$$\beta=\left(-\frac{\gamma_1}{12\gamma_2}\right)^{1/2} \tag{52}$$

$$\lambda_s=\frac{(h_1+h_2)^{3/2}}{a_s^{1/2}} \tag{53}$$

$$\eta_s=a_s\cosh^{-2}\left[\frac{\beta}{\lambda_s}(x-c_st)\right] \tag{54}$$

The shape of an internal solitary wave for $N=2$ is found to agree very well with that obtained from KdV theory (Figure 9). In KdV theory, the ratio of water depth and wavelength is assumed to balance to the square root of the ratio of amplitude and water depth, which means that a nonlinear effect balances to a dispersion effect. This assumption is also applied in the Boussinesq-type equations. Therefore, applying $N=2$ for the proposed fully nonlinear SDI equations is expected to be similar to giving the balance of a nonlinear and dispersion effect used in KdV theory and the Boussinesq-type equations. On the other hand, when $N=3$, the shape on an internal solitary wave is found to be more different from that obtained form KdV theory compared with $N=2$. Because of the short wavelength, such as that the ratio of the wavelength and the lower layer

DOI: 10.1002/fld

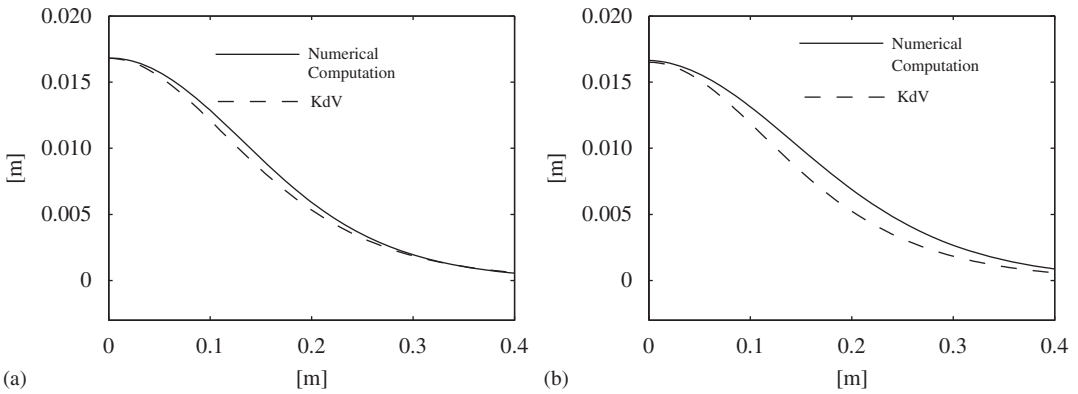

Figure 9. Comparisons of shape of interface displacement for an internal solitary wave. (a) $N=2$ and KdV theory. (b) $N=6$ and KdV theory.

depth is about 10, strong dispersion seems to be needed to reproduce the internal solitary wave investigated in this study.

6. CONCLUSIONS

A new numerical computation scheme is proposed using fully nonlinear SDI equations obtained from variational principle in order to analyze strongly nonlinear and strongly dispersive internal waves. In the proposed numerical computation scheme, run-time cost is expected to be cheaper by solving a matrix for each grid, and the matrix can be solved stably by locating non-zero value in the orthogonal lines.

The proposed numerical computation scheme in this study is revealed to reproduce dispersion relation theoretically obtained from variational principle applying linear assumption. Furthermore, as a result of the comparison of dispersion relation between the small amplitude internal waves and linearlized strongly dispersive internal waves based on variational principle, the proposed equations are found to be applied for reproducing internal waves excluding deepwater waves by taking into account $N=6$ even in the case when the ratio of the depth of the upper and lower layer is 9 for internal waves. For the internal wave case when the ratio of the depth of the upper and lower layer is one and the surface wave case, $N=6$ is found to provide very good agreement with the theoretical solution including strong dispersion cases.

The investigation of an internal solitary wave was conducted up to $N=6$, and a separated internal solitary wave is revealed to propagate in the cases of N is larger than 2. In this study, it is shown that $N=4$ is at least needed to reproduce internal waves. Squared functions are found to be needed to generate velocity potential around an internal solitary wave, which indicates that $N=3$ is at least needed to be included in the numerical computation. Furthermore, it is found from the comparison with KdV theory that the balance of nonlinear and dispersion when $N=2$ is similar to the balance applied in KdV theory and the Boussinesq-type equations.

The proposed numerical computation model is found to reproduce internal waves including higher-order nonlinear effect, which is expected to be applied to clarify the mechanism of high frequency strongly nonlinear internal waves with strong dispersion.

DOI: 10.1002/fld

REFERENCES

1. Antenucci JP, Imberger J, Saggio A. Seasonal evolution of the basin-scale internal wave field in a large stratified lake. *Limnology and Oceanography* 2000; **45**:1621–1638.
2. Antenucci JP, Imberger J. Energetics of long internal gravity waves in large lakes. *Limnology and Oceanography* 2001; **46**:1760–1773.
3. Kakinuma T, Nakayama K. A numerical study on internal waves induced by a typhoon around a continental shelf. *SUISUI Hydrological Research Letters* 2007; **1**:1–4.
4. Hakanson L. Bottom dynamics in lakes. *Hydrobiologia* 1982; **9**:9–22.
5. Ostrovsky I, Yacobi YZ, Walline P, Kalikhman I. Seiche-induced mixing—its impact on lake productivity. *Limnology and Oceanography* 1996; **41**:323–332.
6. Ostrovsky LA, Stepanyants YA. Do internal solitons exist in the ocean? *Reviews of Geophysics* 1989; **27**:293–310.
7. Huthnance JM. Internal tides and waves near the continental shelf edge. *Geophysical and Astrophysical Fluid Dynamics* 1989; **48**:81–106.
8. Winters KB, Peter NR, James JD, Eric A. Available potential energy and mixing in density-stratified fluids. *Journal of Fluid Mechanics* 1995; **289**:115–128.
9. Nakayama K. Comparisons of using CIP, compact and CIP-CSL2 schemes for internal solitary waves. *International Journal for Numerical Methods in Fluids* 2006; **51**:197–219.
10. Okada T, Nakayama K. Modeling of dissolved oxygen in an enclosed bay with sill. *Journal of Environmental Engineering* (ASCE) 2007; **133**(4):447–453.
11. Holloway PE, Pelinovsky E, Talipova T, Barnes B. A nonlinear model of internal tide transformation on the Australian North West Shelf. *Journal of Physical Oceanography* 1997; **427**:871–898.
12. Horn DA, Imberger J, Ivey GN. The degeneration of large-scale interfacial gravity waves in lakes. *Journal of Fluid Mechanics* 2001; **434**:181–207.
13. Choi W, Camassa R. Fully nonlinear internal waves in a two-fluid system. *Journal of Fluid Mechanics* 1999; **396**:1–36.
14. Tomasson GG, Melville WK. Geostrophic adjustment in a channel: nonlinear and dispersive effects. *Journal of Fluid Mechanics* 1992; **241**:23–57.
15. Funakoshi M, Oikawa M. Long internal waves of large amplitude in a two-layer fluid. *Journal of the Physical Society of Japan* 1986; **55**(1):128–144.
16. Matsuno Y. Properties of conservation laws of nonlinear evolution equations. *Journal of the Physical Society of Japan* 1990; **59**(9):3093–3100.
17. Matsuno Y. A unified theory of nonlinear wave propagation in two-layer fluid systems. *Journal of the Physical Society of Japan* 1993; **62**(6):1902–1916.
18. Gerkema T, Zimmerman JTF. Generation of nonlinear internal tides and solitary waves. *Journal of Physical Oceanography* 1995; **25**:1081–1094.
19. Grimshaw R. The solitary wave in water of variable depth. *Journal of Fluid Mechanics* 1970; **42**(3):639–656.
20. Horn DA, Redekopp LG, Imberger J, Ivey GN. Internal wave evolution in a space-time varying field. *Journal of Fluid Mechanics* 2000; **424**:279–301.
21. Kakinuma T. A set of fully nonlinear equations for surface and internal gravity waves. *Proceedings of the 5th International Conference on Computer Modelling of Seas and Coastal Regions*. WIT Press: Southampton, 2001; 225–234.
22. Luke JC. A variational principle for a fluid with a free surface. *Journal of Fluid Mechanics* 1967; **27**:395–397.
23. Isobe M. Time-dependent mild-slope equations for random waves. *Proceedings of the 24th International Conference on Coastal Engineering*. ASCE: New York, 1995; 285–299.
24. Michallet H, Ivey GN. Experiments on mixing due to internal solitary waves breaking on uniform slopes. *Journal of Geophysical Research* 1999; **104**:13467–13477.

DOI: 10.1002/fld